AIAA SciTech Forum
8–12 January 2018, Kissimmee, Florida
2018 AIAA Aerospace Sciences Meeting

10.2514/6.2018-0812

Effects of Flapping Waveforms on the Performance of Burst-and-Coast Swimming in Viscous Flows

Junshi Wang*, Pan Han†, Xiaolong Deng‡, Haibo Dong§
Department of Mechanical & Aerospace Engineering,
University of Virginia, Charlottesville, VA 22904

Emre Akoz**, and Keith W. Moored††,
Lehigh University, Bethlehem, PA 18015

The mechanisms behind bio-inspired propulsion could offer more actuation design strategies for the design of underwater propulsive systems. Recent research has revealed the performance benefit of intermittent swimming comparing to continuous swimming in underwater propulsion. In the current study, we continue our effort on computational analysis of wake structures and performance of a self-propelled hydrofoil under different types of flapping waveforms in viscous flows. An in-house immersed-boundary-method-based flow solver is used to measure the foil performance and associated wake structures. The results indicate that the wake structures of the self-propelled hydrofoils are significantly different from that found in continuous swimming and among different flapping waveforms, which could result in different hydrodynamic performance. Understanding the physics behind the hydrodynamic performance and vortex dynamics may help people to design better bio-inspired underwater vehicle with better swimming strategy.

Nomenclature

θ	Pitching angle
$\overline{U}$	Time-averaged swimming speed
$\overline{T}$	Time-averaged thrust
$\overline{P}$	Time-averaged power
C_T	Coefficient of thrust
CoT	Cost of transport
$\widehat{CoT}$	Normalized cost of transport

I. Introduction

To generate thrust and effectively move in water, aquatic animals have evolved a wide diversity of propulsive mechanisms both in continuous or burst-and-coast locomotion. Numerous studies and models have suggested that those underwater propulsion systems can save as much as 50% of their energy by adopting the burst-and-coast swimming [1-6]. Recently, the inviscid and viscous energy saving mechanisms of coasting phase between bursting

* PhD Student, Department of Mechanical & Aerospace Engineering, University of Virginia, VA 22904, AIAA Student Member.
† PhD Student, Department of Mechanical & Aerospace Engineering, University of Virginia, VA 22904, AIAA Student Member.
‡ Research Scientist, Department of Mechanical & Aerospace Engineering, University of Virginia, VA 22904, AIAA Senior Member.
§ Associate Professor, Department of Mechanical & Aerospace Engineering, University of Virginia, VA 22904, AIAA Associate Fellow.
** PhD Student, Department of Mechanical Engineering and Mechanics, Lehigh University, Bethlehem, PA, 18015.
†† Assistant Professor, Department of Mechanical Engineering and Mechanics, Lehigh University, Bethlehem, PA, 18015.

cycles have been studied using a 2D pitching foil undergoing sinusoidal pitching motion[7]. It is found that the overall performance could be potentially improved for the hydrofoil when using the intermittent swimming strategy. Results have also shown the connection between the foil performance and complex wake structures in viscous flows. In the current study, we further study the hydrodynamics of a 2D pitching foil using different types of the wave forms for burst-and-coast free swimming. Quantitative measurement of foil performance including propulsion force and cost of transportation (CoT) and associated wake structures in all complexity are conducted by using an immersed-boundary-method-based in-house CFD solver[8]. From a fundamental point-of-view, it would be useful to analyze the wake dynamics for non-continuous flapping foils *vis-a-vis* what is known regarding continuous flapping motion.

II. Governing Equation and Numerical Method

The equations solved are the incompressible Navier-Stokes equations, written in indicial form as

$$\frac{\partial u_i}{\partial x_i} = 0; \quad \frac{\partial u_i}{\partial t} + \frac{\partial u_i u_j}{\partial x_j} = -\frac{\partial p}{\partial x_i} + \frac{1}{\mathrm{Re}} \frac{\partial^2 u_i}{\partial x_j \partial x_j} \tag{1}$$

where the indices, i = 1,2,3, represent the x, y and z directions, respectively; p is pressure, u is velocity. The equations are non-dimensionalized with the appropriate length and velocity scales where Re represents the Reynolds number.

A finite-difference based Cartesian grid immersed boundary solver [8] has been developed which allows us to simulate flows with complex immersed 3-D moving bodies. The key feature of this method is that simulations with complex boundaries can be carried out on stationary non-body conformal Cartesian grids and this eliminates the need for complicated re-meshing algorithms that are usually employed with conventional Lagrangian body-conformal methods. The Eulerian form of the Navier-Stokes equations is discretized on a Cartesian mesh and boundary conditions on the immersed boundary are imposed through a "ghost-cell" procedure[8,9]. The method also employs a second-order center-difference scheme in space and a second-order accurate fractional-step method for time advancement. The code has been verified and applied in many flow-structure interaction problems [10-16].

III. Configuration and Simulation Results

In this section, firstly the foil configuration and modeling approach are discussed, then a sequence of numerical simulations are shown to explore the hydrodynamic performance of burst-and-coast pitching. Following these work, the effects of pitching angle shape, and duty cycle period on the foil performance will be examined.

A. Foil Configuration and Kinematics

The configuration of this study is shown in Fig. 1. It includes a 2-D pitching foil, which oscillates in the burst phase in a given motion and then keeps pitching angle 0° in the coast phase. The applied pitching angle shapes vary from triangular shape to step shape. Similar to Akoz et al.[7], Dong et al.[17], Buren et al.[18] and Berman & Wang[19], for the burst pitching motion of the leading edge of the hydrofoil, the triangular pitching angle shape is defined as

$$\theta(t) = y_s(t) \frac{\theta_0}{\arcsin K} \arcsin\left[K \sin\left(2\pi f t\right)\right], \tag{2}$$

where $0 < K < 1$ is a constant in each case. When $K = 0$, it becomes sinusoidal; when $K = 1$, it is triangular waveform. To mimic the step motion, a hyperbolic function is applied

$$\theta(t) = y_s(t) \frac{\theta_0}{\tanh C_\eta} \tanh\left[C_\eta \sin\left(2\pi f t\right)\right], \tag{3}$$

when C_η = 0, θ is sinusoidal; when C_η goes to infinity, $\theta(t)$ tends to be a step function. In Eq. (2) and Eq. (3), $y_s(t)$ is a function for smooth connection

$$y_s(t) = \begin{cases} -\tanh\left(kt\right)\tanh\left[k(t-1)\right], & DC < 1 \\ 1, & DC = 1 \end{cases} \tag{4}$$

In the above equations, θ_0 is the maximum pitching angle, f is the oscillation frequency, and t is the time. In the

current work, $f = 1, k = 30, \theta_0 = 15^\circ$.

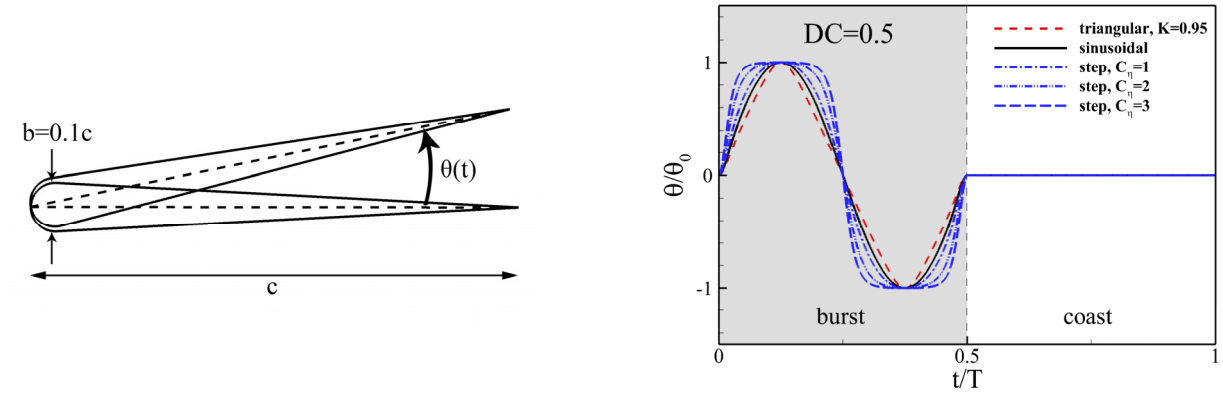

(a) **(b)**

Figure 1. Geometry and pitching motion for the hydrofoil. A hydrofoil undergoing pitching motion (a), and pitching angle waveform defined in burst and coast phases, respectively (b).

Unit length is used for the chord length. The maximum thickness of the airfoil is set to be 10% of its chord length. The ratio of bursting to coasting is controlled by the duty cycle parameter,

$$DC = \frac{burst\ period}{total\ cycle\ period} \tag{5}$$

The foil is pitched with respect to its leading edge. The total period of motion includes a burst phase and a coast phase. The burst phase can be any one pitching motion as described by Eq. (2) or Eq. (3). In the following coast phase, the pitching angle is fixed as $\theta = 0°$. The total cycle period equals the burst period plus the coast period. In current study, DC = 0.5 and 1.0 are chosen, that means the burst phase and coast phase take same period and continuous swimming, respectively.

The simulations are set to be free swimming in x direction and fixed in y direction. After started running, the simulations will take some time to reach steady state, then the mean velocity $\overline{U}$ can be calculated; the mean thrust $\overline{T}$ can be calculated by integrating pressure forces; the mean power $\overline{P}$ can be calculated from the force vector and velocity vector of each boundary element. Following Akoz et al.[7], the cost of transport is defined as

$$\overline{CoT} \equiv \frac{\overline{P}}{m\overline{U}}, \tag{6}$$

the thrust coefficient is defined as

$$\overline{C}_T = \frac{\overline{T}}{0.5\rho S_p \overline{U}^2}, \tag{7}$$

and the power coefficient is defined as

$$\overline{C}_P = \frac{\overline{P}}{0.5\rho S_p \overline{U}^3}. \tag{8}$$

Here S_p is the propulsor surface area. The efficiency is defined as:

$$\eta = \frac{\overline{C}_T}{\overline{C}_P} \tag{9}$$

B. Numerical setup and parameters

In this study, the non-dimensional parameters of Reynolds number and Strouhal number are defined as

$$Re_{\overline{U}} = \frac{\overline{U}c}{\nu}, St_{\overline{U}} = \frac{fA}{\overline{U}}, \tag{10}$$

where ν denotes the kinematic viscosity. $A = 2c\sin\theta_0$ stands for the peak-to-peak amplitude of the trailing edge of the foil.

In the numerical setup, applying a standard referencing velocity $U_{ref} = 1$. Re_{ref} and St_{ref} are given accordingly to determine ν and f. **Error! Reference source not found.**I provides a summary of all the parameters involved in this study and their ranges.

Table I. Parameters involved in the current study and their ranges

Re_{ref}	St_{ref}	DC	θ_0	Triangular Wave	Sinusoidal Wave	Step Wave
2500	0.518	0.5, 1.0	15°	K=0.95	K=0	C_η=1, 2, 3

Validation of the code on plate flapping can be found in previous works [20] . For this particular simulation of flapping foil undergoing burst-and-coast motion, comprehensive grid and domain size independence studies have also been conducted. Based on these studies, a Cartesian grid with a domain size of $30c \times 12c$ and a grid size of 2721×289 have been chosen for all 2-D simulations. The zero-gradient boundary condition is applied to allow the convection of the vortices at all boundaries without significant reflection. The homogeneous Neumann boundary condition is used for the pressure at all boundaries. The no-slip boundary condition is applied to the surface of the foil.

C. Simulation Results

Performance Comparison

Firstly, simulations are performed with fixed DC, fixed θ_0, and changing pitching angle waveforms. One triangular waveform with $K = 0.95$, one sinusoidal waveform, and three step waveforms with C_η = 1, 2, 3 are applied. There are obvious differences among the gradients of θ ($\dot{\theta}$) at 0.25T of these cases, as shown in Table II. For those intermittent swimming cases, the triangular waveform has the minimum $\dot{\theta}$, and then, sinusoidal waveform. All these three step waveforms are characterized with large $\dot{\theta}$, which increases with C_η. And when $C_\eta = 3$, a $\dot{\theta}$ as large as 4.959 can be achieved.

Table II. Angular velocity of pitching foil at 0.25T for intermittent swimming with different waveforms

Waveform	Sinusoidal Continuous	Triangular K = 0.95	Sinusoidal	Step C_η = 1	Step C_η = 2	Step C_η = 3
$\dot{\theta}$ (rad/T_{burst})	N/A	1.247	1.646	2.160	3.412	4.959

Table III shows the comparison of simulation results with different waveforms. Corresponding plots can be found in Figure 2. It can be found that, both $\overline{U}$ with respect to $\dot{\theta}$, and $\overline{CoT}$ with respect to $\overline{U}$, have a quasilinear relationship. With fixed DC and fixed θ_0, when $\dot{\theta}$ increases, the mean velocity will also increase, accompanied with an increasing $\overline{CoT}$, which implies lower efficiency. Comparing to the continuous case (sinusoidal waveform without coasting period), triangular and sinusoidal waveform cases, as well as step waveform case with $C_\eta = 1$, consume less power to move the same distance with the continuous case, while they may take a longer time. In all these cases, the triangular waveform case has the lowest $\overline{CoT}$, which is about half of the continuous case, though the mean velocity is decreased by about 19%. For the sinusoidal waveform case, compared with the continuous case, 18% decrease in mean velocity can be found, while the $\overline{CoT}$ is decreased by about 38%. It is found that the

swimmer here can get a large energy benefit by sacrificing a little bit mean velocity. For the intermittent swimming here to reach the same mean velocity with the continuous case, the burst-coast waveform should be step with C_η which is close to 2, and in this situation, the $\overline{CoT}$ will be increased significantly. This part shows that, by using triangular or sinusoidal waveform intermittent swimming, with deliberate burst-coast arrangement, swimmers can reach a similar mean velocity while using much less energy, when compared with sinusoidal continuous swimming.

Table III. Comparison of time-averaged hydrodynamic performances with different waveforms

Waveform	Sinusoidal Continuous	Triangular $K = 0.95$	Sinusoidal	Step $C_\eta = 1$	Step $C_\eta = 2$	Step $C_\eta = 3$
$\overline{U}\,(c/T_{burst})$	2.487	2.005	2.037	2.104	2.416	2.723
$\overline{CoT}$	2.09	0.986	1.3	1.76	3.13	5.22

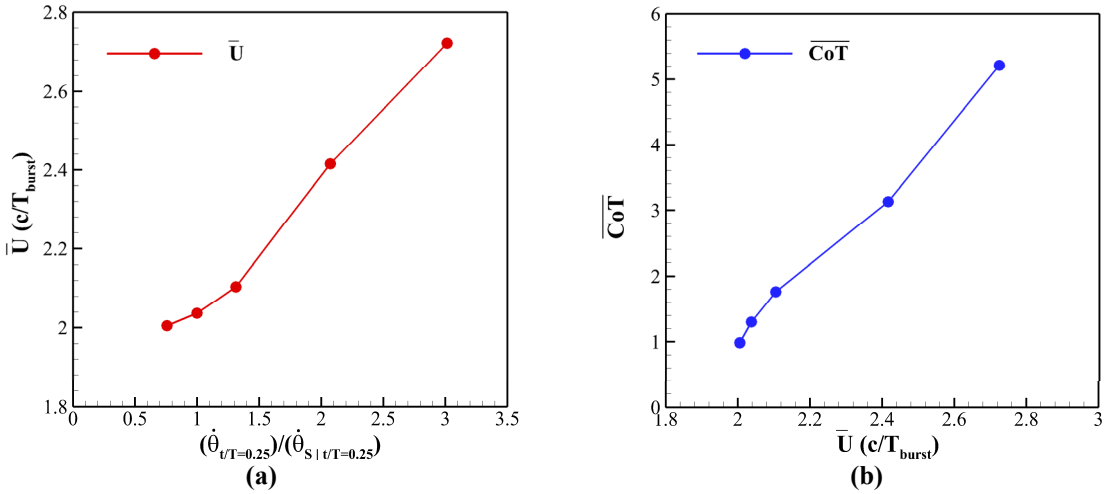

Figure 2: Change of time-averaged swimming velocity $\overline{U}$ (a) and cost of transport $\overline{CoT}$ (b) with different waveforms. $\dot{\theta}_{S|t/T=0.25}$ denotes the angular velocity of the pitching foil at 0.25T in sinusoidal intermittent swimming.

Wake Dynamics

The wake structures generated by the free-swimming pitching foil at are analyzed in this section. The effect of duty cycle (DC) and waveform on the formation of the vortex wake are studied, respectively.

Figure 3 illustrates the comparison of instantaneous wake structures between continuous sinusoidal wave and intermittent sinusoidal wave at DC = 0.5. Three snapshots of the fluid field were taken at 0.0T (Fig. 3a and 3b), 0.5T (Fig. 3c and 3d), and 1.0T (Fig. 3e and 3f) of the second period of the free swimming for both the continuous and the intermittent swimming cases, respectively. For the continuous swimming, the three timings correspond to the start of the first flapping cycle (0.0T), the end of the first fapping cycle (0.5T), and the end of the second flapping cycle (1.0T), respectively, while for the intermittent swimming with DC = 0.5, they correspond to the start of the burst stage (0.0T), the end of burst stage (0.5T), and the end of coast stage (1.0T), respectively. The vortices in the wake are categorized based on the stage when the vortices are shed from the foil. For the continuous swimming, the vortices are grouped by flapping cycles (first and second) and swimming periods (previous and current). For example, the group of vortices shed during the first flapping cycle of the current swimming period T is denoted as FC. For the intermittent swimming with DC = 0.5, the vortices are categorized by swimming gaits (burst and coast) and swimming periods (previous and current). For example, the group of vortices shed during the coast stage of the previous period is denoted as CC. It is found at the three time of the continuous swimming (Fig. 3a, 3c, and 3e), the vortex structures generated in the vicinity of the foil are almost identical, which is due to the periodic flapping motions. Moreover, after these near-field vortices are shed from the foil, their corresponding wake groups SP, FC

and CS are also highly similar. As SP develops, two major vortex pairs (P1 and P2) with vorticity of opposite signs between pairs and same sign within pairs are formed associated with minor vortex pairs. The domain area taken by SP also expends significantly as it develops. For FC, highly similar pattern as SP is observed in the development and expending of the vortex group. As a result, four major vortex pairs (P1, P2, P3, and P4) is generated in the wake of a continuous swimming foil during two consecutive flapping cycles. For the intermittent swimming (Fig. 3b, 3d, and 3f), since the two consecutive swimming stages (burst and coast) are no long the same, the near-field vortices are significantly different at the end of the two stages (e.g., 0.0T and 0.5T). For the same reason, the vortex wake shed during the two stages are also different. It is found during the coast stages (CP and CC), only one major single (S1) is formed associated with minor vortices. However, during the burst stage, two major vortex pairs (P2 and P3) are formed associated with one major single vortex (S2). The signs of vorticity are opposite within P2 and are the same within P3. As a result, two major vortex pairs (P1 and P2) and two major single vortices (S1 and S2) are generated in the wake of an intermittent swimming foil during the two-consecutive burst and coast stages. The domain area of the wake generated within one complete swimming period of the intermittent swimming is smaller than that in the continuous swimming. For the comparison, it is obvious that the foil under continuous swimming gait travels faster than that in the intermittent swimming.

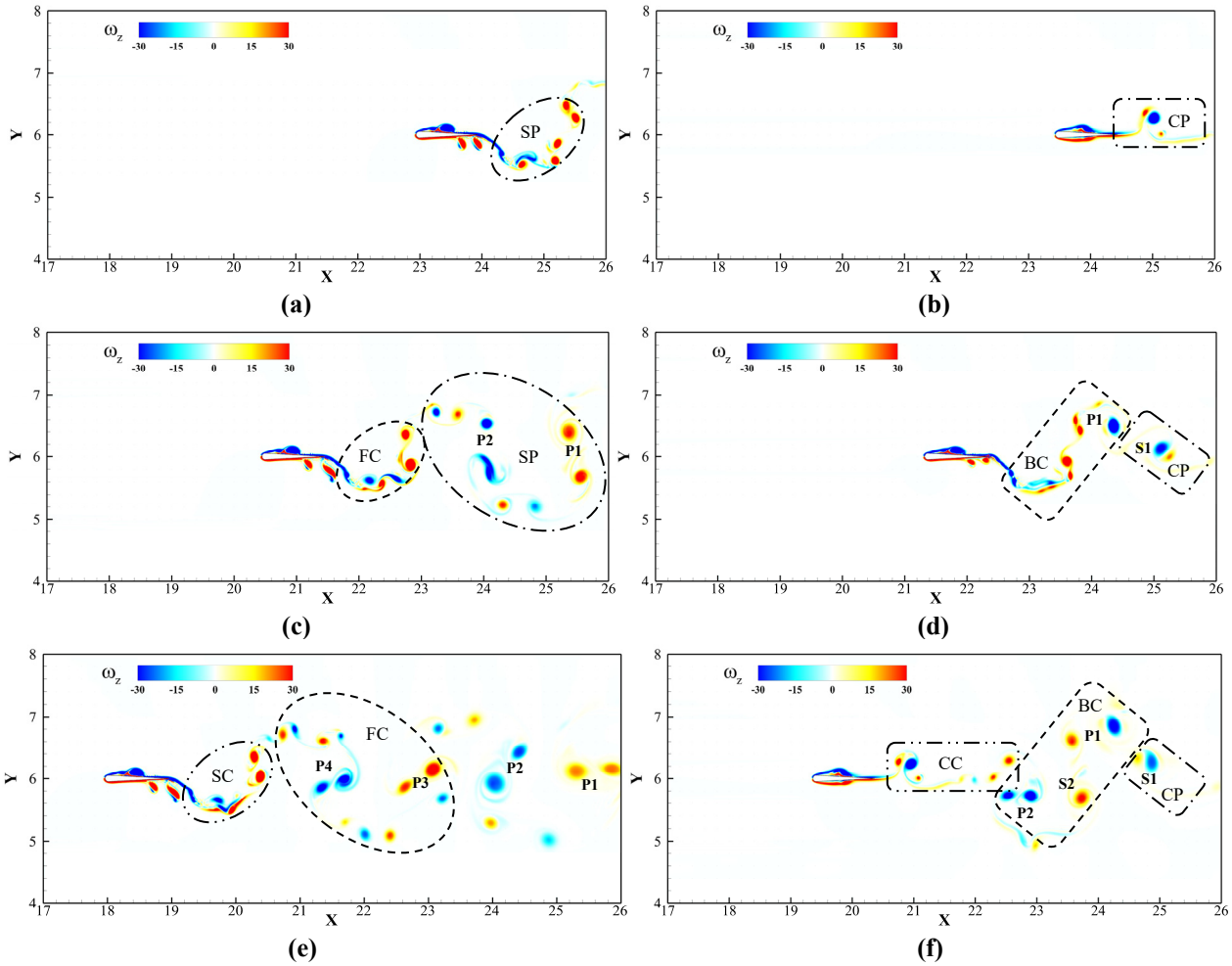

Figure 3: Comparison of wake structures between continuous (a, c, and e) and intermittent (b, d, and f) swimming with DC = 0.5 at t/T = 0, 0.5, and 1.0, respectively, during the second swimming period. The vortex structures are indicated by vorticity ωz.

Figure 4 illustrates the comparison of instantaneous wake structures between different waveforms in intermittent sinusoidal wave at DC = 0.5. The vortex wake generated during the current swimming period is bounded with

dished line. The topology of vortex wake of triangular waveform (TW) and sinusoidal wave (SW) share similar pattern. The TW wake contains four vortex pairs (P1, P2, P3, and P4) and a single vortex (S2) with an overall chronology pattern of PSPPP, while the SW wake contains three vortex pairs (P1, P2, and P3) and two single vortices (S1 and S2) with an overall pattern of PSPSP in chronological order. The vortex wake of the step waveform (ST) shows significant difference from the TW and SW wakes. It is obvious that the ST wake extends to a longer domain and results in stronger vortices than that of TW and SW. Moreover, the ST wake contains two pairs of counter-rotating vortices (P3 and P4) during the coast stage, one more pair than that of TW and SW, making the overall pattern to be SSPPP.

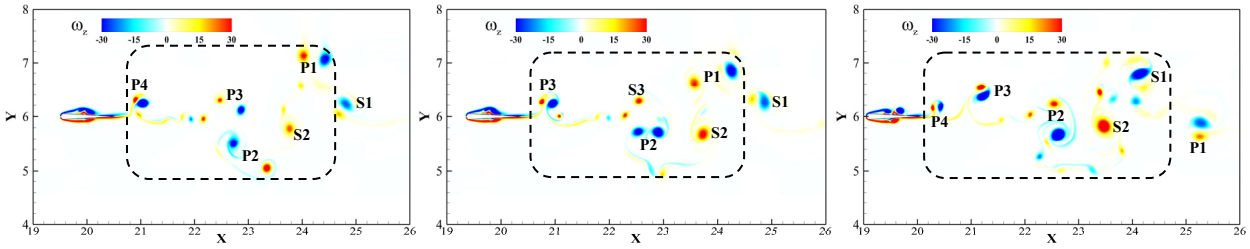

(a) **(b)** **(c)**

Figure 4: Comparison of wake structures between different waveforms (a: triangular wave with K = 0.95, b: sinusoidal wave, and c: step wave with C_η = 1) in intermittent swimming with DC = 0.5 at t/T = 1.0, respectively, during the second swimming period.

IV. Summary

In this paper, numerical simulations of a 2D pitching foil with different waveforms in continuous and intermittent swimming have been conducted using an immersed boundary solver. It is found the continuous swimming gait can achieve a higher swimming speed while consume more energy per distance traveled than that of the intermittent swimming in sinusoidal waveform. By comparing different swimming waveforms in intermittent swimming, it is found the triangular waveform has the advantage of less energy consumption at a lower speed than that of the sinusoidal waveform. On the country, the step waveform can achieve higher swimming speed, but costs more energy per distance traveled than that in the sinusoidal waveform. Significant difference in vortex pattern and strength is found between the wake structure of the continuous and intermittent swimming foil as well as intermittent swimming with different waveforms. Understanding the physics behind the hydrodynamic performance and vortex dynamics may help people to design better bio-inspired underwater vehicle with better swimming strategy.

V. Acknowledgement

This work is supported by the Office of Naval Research under Program Director Dr. B. Brizzolara, MURI Grant Number N00014-14-1-0533, NSF grant CBET-1313217, and NSF grant CBET-1605434.

VI. References

1. Wu G, Yang Y, Zeng L (2007) Kinematics, hydrodynamics and energetic advantages of burst-and-coast swimming of koi carps (Cyprinus carpio koi). Journal of Experimental Biology 210: 2181-2191.
2. Videler J, Weihs D (1982) Energetic advantages of burst-and-coast swimming of fish at high speeds. Journal of Experimental Biology 97: 169-178.
3. Videler J. Swimming movements, body structure and propulsion in cod Gadus morhua; 1981. pp. 1-27.
4. Muller U, Stamhuis E, Videler J (2000) Hydrodynamics of unsteady fish swimming and the effects of body size: comparing the flow fields of fish larvae and adults. Journal of Experimental Biology 203: 193-206.
5. Chung M (2009) On burst-and-coast swimming performance in fish-like locomotion. Bioinspiration & biomimetics 4: 036001.

6. Fish FE, Lauder GV, Mittal R, Techet AH, Triantafyllou MS, et al. Conceptual design for the construction of a biorobotic AUV based on biological hydrodynamics; 2003. pp. 24-27.
7. Akoz E, Liu G, Han P, Dong H, Moored K. Disentangling the Inviscid and Viscous Energy Saving Mechanisms of Intermittent Swimming; AIAA-2017-3981, 47th AIAA Fluid Dynamics Conference, Denver, Colorado, 2017.
8. Mittal R, Dong H, Bozkurttas M, Najjar F, Vargas A, et al. (2008) A versatile sharp interface immersed boundary method for incompressible flows with complex boundaries. Journal of computational physics 227: 4825-4852.
9. Dong H, Mittal R, Bozkurttas M, Najjar F (2005) Wake structure and performance of finite aspect-ratio flapping foils. AIAA Paper 81: 2005.
10. Liang Z, Dong H, Wei M. Computational analysis of hovering hummingbird flight; AIAA-2010-555, 48th AIAA Aerospace Sciences Meeting Including the New Horizons Forum and Aerospace Exposition, Orlando, Florida, 2010.
11. Wan H, Dong H, Huang GP (2012) Hovering hinge-connected flapping plate with passive deflection. AIAA journal 50: 2020-2027.
12. Wang J, Li C, Ren Y, Dong H. Effects of Surface Morphing on the Wake Structure and Performance of Flapping Plates; AIAA-2017-3643, 47th AIAA Fluid Dynamics Conference, Denver, Colorado, 2017.
13. Li C, Wang J, Dong H. Proper Orthogonal Decomposition Analysis of Flapping Hovering Wings; AIAA-2017-0327, 55th AIAA Aerospace Sciences Meeting, Grapevine, Texas, 2017.
14. Han P, Liu G, Ren Y, Dong H. Computational Analysis of 3D Fin-Fin Interaction in Fish's Steady Swimming; FEDSM2016-7699, pp. V01AT04A006, American Society of Mechanical Engineers, Washing, DC, 2016.
15. Bode-Oke AT, Zeyghami S, Dong H (2017) Aerodynamics and flow features of a damselfly in takeoff flight. Bioinspiration & Biomimetics 12: 056006.
16. Ren Y, Liu G, Dong H. Effect of surface morphing on the wake structure and performance of pitching-rolling plates; 2015. pp. 5-9.
17. Dong H, Liang Z, Harff M (2009) Optimal Settings of Aerodynamic Performance Parameters in Hovering Flight. International Journal of Micro Air Vehicles 1: 173-181.
18. Van Buren T, Floryan D, Quinn D, Smits A (2017) Nonsinusoidal gaits for unsteady propulsion. Physical Review Fluids 2: 053101.
19. Berman GJ, Wang ZJ (2007) Energy-minimizing kinematics in hovering insect flight. Journal of Fluid Mechanics 582: 153-168.
20. Li C, Dong H, Liu G (2015) Effects of a dynamic trailing-edge flap on the aerodynamic performance and flow structures in hovering flight. Journal of Fluids and Structures 58: 49-65.